Scattering Dynamics and Kinetic Modeling of CN + H_2 Reactions Across Interstellar Conditions

Faaeze Younesi[a] and Shapour Ramazani[a,*]

a. Department of Chemistry, Yasouj University,7493475918 Yasouj, Iran.

* Corresponding author: ramazani@yu.ac.ir

Keywords

Molecular Dynamics;
Interstellar Medium;
Reaction Probability;
Cross Section;
Scattering Angle.

Abstract

This study examines the dynamics of collisions between the cyano radical CN and molecular hydrogen H2, as well as their deuterated isotopologues. The investigation employs an interpolated potential energy surface derived from QCISD(T)/6-311++G(d,p) ab initio calculations. Classical trajectory simulations were used to evaluate reaction probabilities and cross sections across a broad range of energies. These quantities were analyzed as functions of fragment translational energy, thereby facilitating the examination of how varying energy inputs affect the probability and efficiency of reaction pathways. To better understand the fundamental dynamics of collisions, we investigated the outcomes of inelastic collisions. This examination focused on the redistribution of the initial kinetic energy, analyzing whether it remained conserved as translational motion or was converted into the internal energy of the reaction products. Furthermore, the relationship between the deflection angles and both the impact parameter and the relative translational energy of the colliding entities was evaluated. Rate constants were determined from the calculated cross sections using nonlinear least-squares fitting, thereby enabling the development of quantitative models to characterize the observed kinetics. The investigation of the isotope effect was conducted by substituting deuterium for hydrogen. A method in which the effects of target and incident molecules' mass on cross sections, reaction probabilities, scattering angles, and overall reaction rates are clarified. This comprehensive approach provided an in-depth analysis of the factors influencing collisions between the cyano radical and molecular hydrogen and its isotopic variants.

1. Introduction

Interstellar space is not devoid of matter; it contains various molecules, such as diatomic hydrogen H_2. In addition, nitric oxide HNO, Hydroxyl OH, Carbon monoxide CO, and cyanide CN^- have been identified in the interstellar medium (ISM) [1,2]. Despite the apparent simplicity of these molecules, considerable controversy remains regarding the chemical and physical properties of the interstellar medium. The temperature of the interstellar medium ranges from approximately 10-10^6 K [3,4]. The presence of reactive free radicals, as well as their diverse forms, in combustion and atmospheric processes significantly complicates the underlying chemistry involved [5]. The cyano radical (CN) is one of the most ancient molecular species in the central nervous system and a significant factor in our understanding of space chemistry. Since its identification in the late 1930s in the spectra of nearby stars, this diatomic molecule has garnered considerable attention from astronomers and chemists alike for its utility as a fundamental tool for elucidating the chemical processes that transpire in diverse cosmic environments. The presence of interstellar clouds, regions of low-density gas and dust situated between stars, has captivated the attention of scientists endeavoring to explain the chemical reaction networks that occur in cold and isolated areas of space [6]. Despite numerous methods for producing cyanide over the past several decades, recent studies have demonstrated a promising advance: it is now possible to synthesize CN radicals from atmospheric ammonia under cryogenic conditions. This design primarily advances understanding of interstellar chemistry and provides valuable insights into the chemical evolution of molecular species in cold environments. The investigation of the reaction kinetics and the environmental conditions that facilitate this process clarifies the intricacy of the underlying molecular structure involved [7].

The reactions involving the cyano radical are of substantial practical significance due to its well-documented role in converting fuel-bound nitrogen to nitrogen oxides during combustion. For example, the interaction of cyanide CN^- with hydrocarbons released during the combustion of fossil fuels can produce hydrogen cyanide (HCN), which serves as a crucial precursor in the formation of nitrogen oxides. Nevertheless, despite the importance of this phenomenon, direct measurements of the rate constants for this particular species, especially at elevated temperatures, remain scarce [8]. The cyano radical is a prevalent open-shell species observed in diverse environments, including both the atmosphere and outer space. This compound reacts with small closed-shell molecules via hydrogen abstraction, showing greater reactivity at the carbon atom than at the nitrogen atom. Investigations of specific reactions and their kinetics over the temperature range 100-1000 K have shown excellent agreement with empirical data [7]. The interaction of the cyano radical with molecular hydrogen to generate hydrogen cyanide, along with the subsequent reaction of HCN with atomic oxygen to produce NO, constitutes critical mechanisms in the formation of NO from atmospheric nitrogen and nitrogen-laden fuels [9-11].

The cyano radical is a by-product of the decomposition of nitrogen oxide compounds. The synthesis of hydrogen cyanide through the abstraction of diatomic hydrogen by the cyano radical has been documented at significantly low temperatures, including those prevalent in the interstellar medium. Molecular hydrogen is the most abundant molecule on Earth and plays a major role in the planet's chemical evolution. Hydrogen molecules and their radical forms are important components of extensive molecular clouds and play a crucial role in star formation. Their influence is highly relevant to advancing knowledge in

interstellar chemistry and physics [3]. Despite their relatively straightforward molecular structure, these species demonstrate complicated behaviors when subjected to gravitational forces, temperatures in the vicinity of a few kelvin, and fluctuating electric charges [12,13]. An exploration of the distribution, formation, and chemical properties of H_2 molecules within the interstellar medium may enhance our comprehension of the molecular underpinnings of cosmic evolution. Furthermore, such an investigation might yield basic insights into the chemical processes that lead to the emergence of various molecular species in the cosmos [14,15]. The ground-state H_2 radical is of considerable importance in combustion processes and within the interstellar medium, functioning as a pivotal intermediate that connects simpler atomic species with more intricate molecular structures [16,17].

The investigation of the combustion dynamics of cyano and hydrogen in interstellar space is a critical area of research. This study attempts to clarify the chemical reactions and energy transfer mechanisms occurring in these expansive and complex environments. Such studies are essential for advancing our understanding of the fundamental processes that govern chemical behavior in interstellar media. The process of hydrogen abstraction facilitates the removal of hydrogen atoms in both hydrogen cyanide and hydrogen isocyanide (HNC). Hydrogen cyanide is a major intermediate in hydrocarbon combustion; however, its isomer, HNC, is unstable and seldom encountered in terrestrial environments. The frequency relationship between these two molecules differs significantly. The abundance of HNC is comparable to that of HCN, and in some cases, HNC is more prevalent. The enhanced HNC/HCN ratio is also observed at 1.55 K, which is only 10 K below the carbon compound's reaction threshold [7]. The intrinsic rate coefficients for the reactions of CN(υ=1.0) radicals with O(k_1) and H(k_2)were determined using laser photolysis and laser-induced fluorescence techniques within a heated quartz reactor. The experiments were conducted over a temperature range of 294-1000 K. The information presented herein adheres to the guidelines provided below:

$$k^{TST}(T) = k(T)\frac{K_B T}{h}\frac{Q^T S(T)}{Q^R(T)}\exp(\frac{-DH^{'}}{K_B T})$$

$$k_1(T)_{CN(\upsilon=0)} = (8.7\pm1.0)\times10^{12}\exp\left[+(1.8\pm0.4)\frac{kJ}{RT}\right] \text{cm}^3\ \text{mol}^{-1}\ \text{s}^{-1}$$

$$k_1(T)_{CN(\upsilon=1)} = (8.4\pm1.2)\times10^{-12}\exp\left[+(1.2\pm0.4)\frac{kJ}{RT}\right]\ \text{cm}^3\ \text{mol}^{-1}\ \text{s}^{-1}$$

$$k_2(T)_{CN(\upsilon=0)} = (3.1\pm0.3)\times10^{5}T^{2.45}\exp\left[-(9.3\pm0.2)\frac{kJ}{RT}\right]\ \text{cm}^3\ \text{mol}^{-1}\ \text{s}^{-1}$$

$$k_2(T) = (2.9)\times10^{5}T^{2.45}\exp\left[-(9.36)\frac{kJ}{RT}\right]\ \text{cm}^3\ \text{mol}^{-1}\ \text{s}^{-1}$$

In the temperature range of 300-1000 K, we applied a curved Arrhenius expression of the form $k = AT^B\exp(-E_a/RT)$, with B set to 2.45 in accordance with theoretical predictions. The aforementioned expression effectively characterizes the temperature range of 295- 3500 K, and the parameters obtained align with those determined through ab initio methodologies [7,18,19]. The rate constant for the reaction between NH and C_2 has been established as $k(T) = 7.85\times10^{7}\times T^{0.8682}$ L mol^{-1} s^{-1}, with an associated activation energy of 60.39. The existing literature suggests that NH and ND are the predominant products generated across all reaction pathways, exhibiting the greatest probability of occurrence [20]. The rate constant for the excitation of NH-OH, ND-OH, NH-OD, and ND-OD was also determined. In the calculation of the rate constant, several structural configurations and potential energy surfaces were assessed that arise from the substitution of hydrogen with deuterium. The rate constants were determined as follows:

$$k(T) = 3.5\times10^{7}\times T^{0.8628}\ \text{L mol}^{-1}\ \text{s}^{-1}$$

$$k(T) = 3\times10^{7}\times T^{0.8728}\ \text{L mol}^{-1}\ \text{s}^{-1}$$

$$k(T) = 4.2\times10^{7}\times T^{0.88278}\ \text{L mol}^{-1}\ \text{s}^{-1}$$

$$k(T) = 1.6\times10^{7}\times T^{0.9318}\ \text{L mol}^{-1}\ \text{s}^{-1}$$

corresponding to an activation energy range of 36.76-131.30 kJ mol^{-1} [21]. Some other investigations were conducted under conditions of temperature ranging from 200-3000 K and 4100-15000 K [22,23]. The chemical interactions between dicarbon and imidogen have garnered significant attention due to their frequent co-occurrence in various combustion processes and extraterrestrial environments. The significance of these reactions is widely acknowledged, and substantial research has been conducted to investigate their rates, particularly in the presence of other molecules. For instance, reactions involving dicarbon and imidogen have been systematically studied using a diverse array of collision partners, including NH, C, C_2, and H_2. In the present study, the dynamics and kinetics of the collision between the cyano radical and molecular hydrogen were investigated.

The principal objectives of this research were: (1) to characterize the potential energy surface (PES) associated with reactions between CN and H_2, (2) to determine the reaction probability cross sections, (3) to analyze isotopic effects to assess the influence of mass, (4) to investigate elastic scattering phenomena, and (5) to compute rate constants.

2. Method

2.1. Computational details

In this study, the potential energy surfaces (PES) associated with the combustion reaction of cyano and dihydrogen were analyzed utilizing the Gaussian 09 computational program [24]. Stationary points were optimized utilizing the Quadratic Coupled-Cluster with Single and Double excitations QCISD method using the 6-311++G(d,p) basis set [25,26]. The angles and bond lengths at all stationary points were optimized and are presented in Figure 1. Figure 2. relative energy profiles for the stationary points of the reaction CN + H_2, corrected for zero-point energy (ZPE), are presented. These profiles were calculated at the QCISD(T)/6-311++G (d,p) level of theory, reflecting the quantum-chemical energy landscape of the reaction pathway. The interaction between the cyano radical and the dihydrogen resulted in the formation of three intermediates: trans-HCNH, cis-HCNH, and H_2CN, as well as the products H + HCN and H + HNC. Additionally, HCN and HNC were generated directly by abstraction of a hydrogen atom from HHCN. H_2 and CN reacted to produce HHCN instantaneously.

$CN+H_2$	Products	(R1)	CN+HD	Products	(R6)
	HCN+H	(R2)		HCN+D	(R7)
	HNC+H	(R3)		HNC+D	(R8)
	trans-HCNH	(R4)		trans-HCND	(R9)
	cis-HCNH	(R5)		cis-HCND	(R10)
CN+DH	Products	(R11)	$CN+D_2$	Products	(R16)
	DCN+H	(R12)		DCN+D	(R17)
	DNC+H	(R13)		DNC+D	(R18)
	trans-DCNH	(R14)		trans-DCND	(R19)
	cis-DCNH	(R15)		cis-DCND	(R20)

2.2. Computation of the potential energy surface

Investigations of reactive or nonreactive chemical processes at the molecular level were conducted with knowledge of the potential energy surface. The nature of a PES could be determined in one of two ways: either experimentally or by the use of an ab initio quantum-mechanical process. Numerous molecular configurations in PES were required to investigate the kinetics of a reaction [27,28]. Collins presented the Growing program, a technique for building molecular PES using traditional trajectory calculations [29,30]. PES was used to create the Grow methodology via a modified Shepard interpolation technique. The specifics of the Grow methodology had already been discussed elsewhere, so we included a synopsis here. PES could be created for a molecule with four or more atoms by utilizing all interatomic distances, $N(N\text{-}1)/2$. Atom–atom distances R_N, $N=1,...,N(N\text{-}1)/2$ was readily calculated from the Cartesian coordinates for any atomic configuration, for example:

$$R_1=\left[(X_1-X_2)^2+(Y_1-Y_2)^2+(Z_1-Z_2)^2\right]^{\frac{1}{2}} \tag{1}$$

R_2 is the distance from atom 1 to atom 3, and $R_{N(N-1)/2}$ is from the atom $N-1$ to atom *N*. Rather than using atom–atom distances, the reciprocal distance Z_N where $Z_N=(1/R_N)$ were used; the PES could be approximated in the vicinity of some configuration Z_i by a Taylor expansion:

$$T_i(Z)=V[Z(i)]+\sum_{K=1}^{3N-6}\left[Z_K-Z_K(i)\right]\frac{\partial y}{\partial Z_K}+\frac{1}{2!}\sum_{K=1}^{3N-6}\sum_{J=1}^{3N-6}\left[Z_K-Z_K(i)\right]\left[Z_J-Z_J(i)\right]\frac{\partial^2 y}{\partial Z_K\partial Z_J}+... \tag{2}$$

This extension could be continued beyond the quadratic differentiation of *Z* with respect to *Z*(*i*). The necessary energy and properties of some N_d (element number) were provided by ab initio quantum chemistry programs, including the Cartesian coordinates $X=(X_{i,i=1,...,3N})$.

According to the Grow formula, the modified Shepard interpolation method can be used to express the potential energy surface as the weighted average of the Taylor expansion of the Z molecular configuration, and is given by:

$$E(Z) = \sum_{i=1}^{N_{data}} W_i(Z) T_i(Z) \tag{3}$$

Here, $T_i(Z)$ was a second-order Taylor expansion of the force around each data point, and the weight $W_i(Z)$ was a function of the distance Z between the data points in the point set Z_i. The complete calculation of the N_{data} geometries, including the potential and first and second derivatives, were evaluated ab initio. For each ab initio energy data point, the gradient and Hessian can be calculated using a Taylor expansion. The working weight was written in the original weight form (V_i):

$$W_i = \frac{V}{\sum_{i=1}^{N_{data}} V_j} \tag{4}$$

$$V_i = \left\| Z - Z_i \right\|^{-p}, p > (3N - 3) \tag{5}$$

The weight function in Eq. (3) was due to the effect of the data on Z_i near Z_i, which changes more rapidly than the potential energy surface, thereby weakening the body in the PES. This problem can be solved by adjusting:

$$V_i = \left\{ \left[\sum_{n=1}^{N(N-1)/2} \frac{(Z_n - Z_n(i))}{d_n(i)} \right]^{\frac{q}{2}} + \left[\sum_{n=1}^{N(N-1)/2} \frac{(Z_n - Z_n(i))}{d_n(i)} \right]^{\frac{p}{2}} \right\}^{-1} \tag{6}$$

$$d_n(i)^{(-6)} = \frac{1}{M} \sum_{j=1}^{M} \frac{\left\{ [\frac{\partial E}{\partial Z_n}] \left| Z(j) - \frac{(\partial T_i)}{(\partial Z_n)} \right|_{Z_j} [Z_n(j) - Z_n(i)] \right\}^2}{E_{tot}^2 \left\| Z_n(j) - Z_n(i) \right\|^6} \tag{7}$$

Where $p > (3N - 3)$ and $q < 2$, but $q \square\ p$. In Eq. (6), $d_n(i)$ played the role of confidence lengths.

3. Results

3.1. Classical dynamics calculations

Subsequent studies have provided comprehensive elucidations of the development of the potential energy surface and quasi-classical trajectory modeling at specific internal translational energies of reactants. These investigations aimed to identify novel data points within critical dynamic regions of the configurational space, thereby facilitating the generation of an accurate and comprehensive PES. Each iteration of the Potential Energy Surface PES structure executes a limited set of 10 trajectories to model the collisions between carbon-nitrogen radicals and hydrogen molecules. The trajectories were determined through the application of the velocity-Verlet integration algorithm with a time step 1×10^{-17} s, starting value of the impact parameter of 0 Bohr. [31]. In the following, the incorporation of a defined number of molecules into the ab initio point pool dataset was followed by an evaluation of the precision of molecular location using quantum scattering calculations. The convergence of response probabilities shows a strong correlation with dataset size.

The total reaction probability versus the data points for the collisions between reactants is shown in Figure 3. As seen, the reaction probability for R1 remained constant from 1200 to 1500 data points, indicating that the PES was converging. This was derived by adding 1422 data points from the box path to the 78 initial data points obtained from an ab initio calculation. A comprehensive collection of 2000 trajectories about reactions between fragments at varying relative translational energies was systematically interpolated across diverse data set sizes. The maximum impact parameter b_{max} and the initial separation were set to 4 Bohr and 5.5 Bohr, respectively, for the reaction probability calculations. Finally, the interpolated PES for a data set of 1800 points was used to determine the reaction probability, cross-sections, and rate constant for reactive and non-reactive collisions.

Figure 4 illustrates the distribution of relative internal energies of the data points in relation to the energy associated with the reactants. The observed peak suggests the most probable energy level, corresponding to the energies of dissociation products such as CNH + H and HNC + H, as well as potentially relevant intermediates. Data points with minimal energy levels are observed in regions where the potential energy surface achieves the highest accuracy. The presence of a limited number of energy states that exceed that of the reactants indicates that the formation of such products is kinetically improbable. The energy range of the data extends from -900 kJ mol^{-1} to 0 kJ mol^{-1} relative to the reactants. While the addition of points does not influence the magnitude of the change, the potential energy surface has been characterized as an approximation. A critical component of this study involved analyzing the dynamic properties of the reactant-type reaction, evaluated over 1500 data points. Quantum

mechanics and quasi-classical dynamics were employed to compute the reaction probability, denoted as P_r. This signifies an advantageous region where the reactants collide and interact. The outcome is contingent upon the quantum states of the molecules involved and the relative velocities of the reactants. Furthermore, the reaction probability P_r was associated with the collision dynamics as determined through classical mechanics analyses.

The collision cross-section of the reaction is the area of a beam molecule observed by the target molecule, which was determined from the collision dynamics calculation as follows:

$$\sigma(E_{tr}) = \pi(b_{\max})^2 P_r \tag{8}$$

P_r is the reaction probability, which is the ratio of the number of reactive trajectories to the total number of trajectories, and is quantitatively expressed by the equation $P_r = N / N_r$, where N and N_r are the total number of all trajectories and the number of trajectories leading to the product, respectively. The maximum impact parameter observed in this reaction b_{max}, was measured to be 5.5 Bohr units. For each trajectory, the parameter b was selected within the range of 0 to 5.5. The initial interparticle distance was measured to be 8 Å. The reaction rate was determined by assessing the initial relative velocity or kinetic energy of the reactant molecules. Figure 5 denotes the reaction probability as a function of the impact parameter, demonstrating a peak at minimal initial values of b. Collisions characterized by impact parameters exceeding 5.5 Bohr demonstrate minimal interaction. A detailed examination of scattering analyses at this threshold will be presented subsequently. The principal distinction between R1 and R15 resides in the mass of the colliding particles, specifically hydrogen H_2, in contrast to deuterium D_2. The greater mass of D_2 is associated with an increased probability of reaction. The overall reaction probability, as determined by trajectory simulations, is influenced by the internal states of both the reactants and products, as well as their respective relative translational energies.

3.2. Effects of fragment mass on observable data of reactions

This section examines the impact of particle mass on reaction rates and product distributions, as documented in the literature [21,32-33]. The translational energy and the mass of the molecules involved influence the dynamics of interactions during molecular collisions. This section evaluates the impact of hydrogen-deuterium exchange by analyzing reactions. Specifically, it examines how the masses of both target and incident molecules affect reaction probabilities, cross-sections, and rates. Reactions R6 and R20 pertain to the substitution of hydrogen with deuterium. Furthermore, the reactions R7-R10, R12-R15, and R17-R20 are identified as subsets of R6, R11, and R16, respectively. Figures 6 and 7 illustrate that the reaction probability and cross-section for reactions involving deuterium are greater than those for reactions involving hydrogen. This phenomenon can be attributed to the fact that, at equivalent relative velocities, heavier particles D interact with the target for a longer duration. This long interaction consequently enhances the probability of a reaction occurring.

3.3. scattering that is not elastic

Numerous collisions did not yield diminished reaction outcomes for this particular interaction (CN and HH); consequently, it was essential to examine the particle distribution using extended observations and low-energy parameters. This collision surpassed the non-merger incident between CN and HH. This energy can be converted into vibrational or rotational modes. In line with comparable studies [34], the collision dynamics exhibited analogous results for carbon nitride CN and hydrogen-hydrogen HH collisions. In this article, a substantial proportion of trajectories for the reaction between NH and OH showed no reactivity. Consequently, this section focuses on the analysis of scattering trajectories. In inelastic collisions, a portion of the internal energy of OH and NH particles is exchanged between the particles or converted into translational energy. Eq. (9) expresses the scattering angle as a function of the impact parameter and the relative translational energy of the collision.

$$\theta(E,b) = \pi - 2b\int_{r_{\min}}^{\infty} \frac{dr}{r^2\left[1-\frac{b^2}{r^2}-\frac{V(r)}{E}\right]^{\frac{1}{2}}} \tag{9}$$

In this study, the variable r denotes the distance between the particles at any given time. The corresponding integral is evaluated over the range from r_{min} to infinity. The parameters b, E and V_r represent the impact parameter, the relative translational energy, and the potential function, respectively, where r denotes the distance between the particles. Furthermore, several studies have indicated a correlation between the classical deflection angle and angular momentum [35]. The association between angle and multiplication can be articulated in the following manner:

$$\theta(E,b) = 2\cos^{-1}(\frac{b}{d}) \tag{10}$$

For $b < d \rightarrow \theta(E,b) = 2\cos^{(-1)}(\frac{b}{d})$ but for $b > d \rightarrow \theta(E,b) = 0$.

The angle was determined by the length range of the negative effect potential, indicating whether positive or negative effects were potentially attractive or unattractive, respectively.

$$\theta(E,b) = \pi - 2\beta \int_{r_0} \rho^2 \left[1 - \frac{w(\rho)}{K} - \frac{\beta^2}{\rho^2} \right]^{-\frac{1}{2}} d\rho \tag{11}$$

Where

$$V(r) = \varepsilon W(\rho) \ , \ \rho = \frac{r}{r_0} \text{ , and } K = \frac{E}{\varepsilon} \ . \tag{12}$$

Suppose the potential was a very important term, for instance, the charge-induced dipole moment in an ion-neutral reaction. In that case, it should be expressed as a good approximation of the long-range intermolecular potential for analysis. The relationship between the angle and the multiplication could then be represented as:

$$\theta = 2\,\text{arccot}\left[\frac{\left(mv_0^2 \big/ K \right)}{b} \right] \tag{13}$$

$$K = k \times q \times Q = 2kZe^2 = (4.6 \times 10^{-28} N.m^2)Z, k = 8.99 \times 10^9 (N.\frac{m^2}{C^2}) \tag{14}$$

In this context, represents the atomic number of the nucleus, while e denotes the charge of the electron. Additionally, m and v_0 denote the mass and initial velocity of the particle, respectively. At multiple scattering angles for the reactions of (H_2, HD, DH, and D_2), the proportion of non-reactive H_2 and D_2 radicals was illustrated in Figure 8 at an energy of 65. 63 kJ mol^{-1}.

The scattering of the attachment particles occurred within the angular range of 0.5 to 3 degrees. The analysis revealed three distinct regions corresponding to the scattering angles. Initially, it is observed that b approaches zero. In this region, the impact parameters were observed to be smaller than d, defined as $d\left(d = \frac{1}{2}(\frac{d_{CN}}{d_{H_2}})\right)$ with the variable b being less than 6. In the context of low-impact parameters, the scattering angle for the reaction showed an indirect dependence on both the impact parameter and the translational energy. However, for certain energy levels exceeding 80 kJ mol^{-1}, an increase in the parameter b was observed to correlate with an increase in impact parameters less than 5.5 Bohr. The second area of investigation pertained to large impact parameters, characterized by $b > d$, in which the colliding particles did not make contact with one another. In this context, a weak inverse relationship was observed between the variables b and θ, which ultimately approaches zero. The value of variable b is greater than 9. Furthermore, there exists a diminished correlation between the scattering angle and the impact parameter within the regime where $b > d$. This observation elucidates why the scattering behavior resembles that of a hard sphere; consequently, the particles experienced minimal scattering due to the rapid attenuation of the attractive component of the Lennard-Jones potential in this region. In the third region, a weak correlation was observed between θ and b, specifically in the range of impact parameters from 6 to 9, alongside the occurrence of collisions at intermediate intervals of these impact parameters.

In Figure 9, for energy values ranging from 40 to 60 kJ mol-1, the scattering angle shows a strong dependence on the impact parameter, decreasing as the impact parameter increases. In Figure 8, the long-range potential observed in the CNH_2 collision study exhibits a relatively flat profile, thereby rendering the generalization of the interaction ambiguous. At low impact values, the scattering angles showed distinct variations with respect to the impact parameters. At large impact parameters, an observed weak inverse correlation exists between the scattering angle and the impact parameter, with the scattering angle remaining constant for $b > 14$. For the range where $7 > b > 5$, the observed behavior exhibited notable differences. In specific trajectories, molecules with identical impact parameters were oriented differently, resulting in deflections at different angles. This phenomenon led to minimal separation distances $6 < b < 9$, thereby resulting in diverse interactions and varying scattering angles. We calculated the mean of these angles for each respective b value. For impact parameters less than 6 Bohr or exceeding 9 Bohr, fitting methodologies were utilized to ascertain the formulas governing the scattering angles, as demonstrated in Table 1.

3.4. Rate constant calculation

The reaction cross-section and the reaction probability are associated and can be calculated from classical mechanics. According to the physically reasonable assumptions and collision theory, for the rate constant, a simple expression could be written as a function of the reaction cross-section $\sigma(E)$ at temperature T. Therefore, a relationship between the quantity and the rate constant $k(T)$, cross-section $\sigma(E)$, and the probability of reaction P_r, and different approaches to the definition of the nuclear dynamics are as follows:

$$k(T)=\left[\frac{8}{\pi\mu(K_BT)^3}\right]^{\frac{1}{2}}\int_0^{\infty}E\sigma(E)\exp\left(-\frac{E}{K_BT}\right)dE \quad (15)$$

where K_B is Boltzmann's constant, μ is the molecule-molecule reduced mass, and E is the translation energy. A power law can express the reaction cross-section:

$$\theta(E)=aE^{\gamma}(\gamma>-2) \quad (16)$$

After substituting Eq. (16) with Eq. (15) and calculating the integral, the rate constant was obtained as:

$$k(T)=a(\frac{8}{\pi\mu})^{\frac{1}{2}}\Gamma(\gamma+2)(K_BT)^{(\gamma+\frac{1}{2})} \quad (17)$$

Here, Γ represented the gamma function. The fitted parameters for calculating the total cross-section, (a, γ, $\Gamma(\gamma+2)$) and $k(T)$ L mol^{-1} s^{-1} for some reactions were shown in Table 2. The rate constant expressions for the R1 and R20 reactions were obtained as follows, consisting of two parts: the first was the pre-exponential factor, and the second was the temperature-dependent part.

To examine how temperature affects the computed rate coefficient, an Arrhenius plot is shown in Figure 10. As illustrated, increasing temperature (or the relative translational energy of reactants) raises the rate constant. The rate constant for the deuterium-involving reaction R1 was higher than that for the hydrogen-based response R1. These findings suggest that the rate constant depends on the mass of the reacting particles. Previously, one of the authors of this paper investigated the primary kinetic isotope effect (KIE) for the reactions of methyl radical with methane and trichloromethyl radical [35]. Since this number is greater than 1, it shows that the reaction rate for hydrogen is higher than that for deuterium when only translational energy is considered. However, deuterium reacts more easily than hydrogen due to other factors like rotational and vibrational energy. As the temperature rises, the translational energy coefficient stays constant, but the relative reaction rate of hydrogen compared to deuterium increases. This is because temperature has a greater impact on the vibrational and rotational energy contributions in hydrogen reactions.

The primary kinetic isotope effect reflects the quantum nature of nuclei and the zero-point energy shift, leading to differences in the vibrationally averaged properties of compounds with lighter and heavier masses. This effect includes vibrational, rotational, and transitional contributions.

$$\frac{k_H}{k_D}=\eta_{tun}\times\eta_{rot}\times\eta_{vib}\times\eta_{trans} \quad (18)$$

$$\eta_{trans}=\frac{(\frac{m^{TS}}{m^{reac\tan t1}}\times\frac{m^{TS}}{m^{reac\tan t2}})_H^{(3/2)}}{(\frac{m^{TS}}{m^{reac\tan t1}}\times\frac{m^{TS}}{m^{reac\tan t2}})_D^{(3/2)})} \quad (19)$$

$$\eta_{rot}=\frac{\frac{Q^{TS}_{(rot.H)}}{Q^{reac\tan t1(CN)}_{(rot.H)}\times Q^{reac\tan t2(H_2)}_{(rot.H)}}}{\frac{Q^{TS}_{(rot.D)}}{Q^{reac\tan t1(CN)}_{(rot.D)}\times Q^{reac\tan t2(H_2)}_{(rot.D)}}} \quad (20)$$

$$\eta_{vib}=\frac{\frac{Q^{TS}_{(vib.H)}}{Q^{reac\tan t1(CN)}_{(vib.H)}\times Q^{reac\tan t2(H_2)}_{(vib.H)}}}{\frac{Q^{TS}_{(vib.D)}}{Q^{reac\tan t1(CN)}_{(vib.D)}\times Q^{reac\tan t2(H_2)}_{(vib.D)}}} \quad (21)$$

In Table 3, the partition function Q refers to the stationary points, and m represents the mass of the species involved. The value of η trans was 1.026 for all energy levels. Presents the results of the isotope effects on the rate constants for the reactions CN + H_2 and CN + D_2, k_1/k_{16}. Deuterated cyano reacts faster than hydrogenated cyano.

4. Conclusions

This study systematically investigates the reaction dynamics of the cyano radical, CN, with molecular hydrogen, H_2, and its isotopologues. This investigation was conducted by developing an interpolated potential energy surface, grounded in ab initio electronic structure calculations, and then applying quasi-classical trajectory simulations. The findings indicate that the

translational energy of the colliding fragments exerts a profound influence on reaction probabilities, cross sections, and scattering behaviors. Also, the introduction of isotopic substitution leads to basic variations in reaction rates, scattering angles, and energy transfer mechanisms. Inelastic collisions demonstrated a partial conversion of translational energy into vibrational and rotational excitations, thereby highlighting the intricate interplay between internal and external degrees of freedom in determining reaction outcomes. Moreover, the isotope effect substantiated the essential influence of molecular mass on collision lifetimes and reactivity, as evidenced by the observation that deuterium-containing systems demonstrated increased reaction probabilities and cross sections. The quantification of rate constants across a broad temperature range facilitates the development of robust kinetic models applicable to both interstellar and terrestrial combustion environments. In anticipation of future developments, several promising avenues for exploration and research emerge from this study. To enhance understanding of tunneling effects and resonant phenomena that may predominate under interstellar conditions, it is essential to extend these simulations to include quantum scattering calculations at ultralow temperatures. Furthermore, the inclusion of more complex hydrogen-containing species, such as hydrocarbons or polyatomic radicals, would enhance the relevance of the current findings within the contexts of combustion chemistry and astrochemical reaction networks. In addition, integrating the current dynamical data with astrochemical kinetic models may elucidate the significance of cyanide-driven pathways in the evolution of molecular clouds and the processes of star formation. Ultimately, experimental verification through sophisticated crossed-beam scattering techniques or time-resolved spectroscopy would serve as essential benchmarks for validating and refining the theoretical framework outlined in the present study. This investigation significantly advances our comprehension of the fundamental dynamics underlying CN-H_2 interactions. Furthermore, it lays a crucial foundation for future research endeavors that seek to bridge the gap between molecular-scale reactivity and macroscopic chemical evolution in both laboratory and astrophysical contexts.

Biographies

Faaeze. Younesi received the MSc degree in Physical Chemistry from the University of Yazd, Iran. She began her PhD studies at Yasouj University under the supervision of Dr. Shapour Ramazani. Her research interests include interstellar reactions and the study of the kinetic isotope effect.

Shapour Ramazani is an Associate Professor at the Chemistry Department of Yasouj University. He obtained his PhD degree from the Chemistry Department of Shiraz University in 2008, followed by a one-year sabbatical period at the Australian National University (Professor Michael Collins's group). His current research interests focus on the kinetics and dynamics of biological reactions.

Reference

1. Kumar, S.S., Grussie, F., Suleimanov, Y.V., et al. “Low temperature rates for key steps of interstellar gas-phase water formation”, *Science Advances*, **4**(6), eaar3417 (2018). https://doi.org/10.1126/sciadv.aar3417
2. Silva, M.X., Mendoza, E., Ferreira, F.S.L., et al. “New routes for PN destruction and formation in the interstellar medium via neutral-neutral gas-phase reactions and an extended database for reactions involving phosphorus”, *Astronomy and Astrophysics*, **696**, A170 (2025). https://doi.org/10.1051/0004-6361/202453204
3. Borget, F., Müller, S., Grote, D., et al. “CN radical hydrogenation from solid H_2 reactions, an alternative way of HCN formation in the interstellar medium”, *Astronomy and Astrophysics*, **598**. A27 (2017). https://doi.org/10.1051/0004-6361/201526383
4. Fredon, A., Radchenko, A.K., and Cuppen, H.M. “Quantification of the role of chemical desorption in molecular clouds”, *Accounts of Chemical Research*, **54**(4), pp. 745-753 (2021). https://doi.org/10.1021/acs.accounts.0c00636
5. Klos, J. and Lique, F. “First rate coefficients for an interstellar anion: Application to the CN-H_2 collisional system”, *Monthly Notices of the Royal Astronomical Societ,* **418**(1), pp. 271-275 (2011). https://doi.org/10.1111/j.1365-2966.2011.19481.x
6. Schulz, A. and Surkau, J. “Main group cyanides: from hydrogen cyanide to cyanido-complexes”, *Reviews in Inorganic Chemistry*, **43**(1), pp. 49-188 (2023). https://doi.org/10.1515/revic-2021-0044
7. Burke, A.D., Bowman, MC., Turney, J.M., et al. “Energetics and kinetics of various cyano radical hydrogen abstractions”, *Physical Chemistry Chemical Physics*, **23**(5), pp. 3389-3400 (2021). https://doi.org/10.1039/d0cp06228f
8. Balla, R.J., Casleton, K.H., and Adams, J.S. “Absolute rate constants for the reaction of CN with CH_4, C_2H_6 and C_3H_8 from 292 to 1500 K using high-temperature photochemistry and diode laser absorption”, *The Journal of Physical Chemistry*, **95**(22), pp. 8694-8701 (1991). https://doi.org/10.1021/j100175a051
9. Sims, I.R., Queffelec, J.L., Travers, D., et al. “Rate constants for the reactions of CN with hydrocarbons at low and ultra-low temperatures”, *Chemical Physics Letters*, **211**(4-5), pp. 461-468 (1993). https://doi.org/10.1016/0009-2614(93)87091-G

10. Wooldridge, S.T., Hanson, R.K., and Craig T.B. "A shock tube study of reactions of CN with HCN, OH, and H_2 using CN and OH laser absorption", *International Journal of Chemical Kinetics*, **28**(4), pp. 245-258 (1996). https://doi.org/10.1002/(SICI)1097-4601(1996)28:4%3C245::AID-KIN2%3E3.0.CO;2-V
11. Rivilla, V.M., Jiménez-Serra, I., Garcí De La Concepción, J., et al. "Detection of the cyanomidyl radical (HNCN): a new interstellar species with the NCN backbone", *Monthly Notices of the Royal Astronomical Society: Letters*, **506**(1), pp. 79-84 (2021). https://doi.org/10.1093/mnrasl/slab074
12. Li, X., Lu, B., Wang, L., et al. "Unraveling sulfur chemistry in interstellar carbon oxide ices", *Nature Communications*, **13**(1), A7572 (2022). https://doi.org/10.1038/s41467-022-349494
13. Jubert, L., Martínez-Bachs, B., Pareras, G., et al. "Energy partitioning in H_2 formation on interstellar carbonaceous grains. Insights from ab initio molecular dynamics simulations", *Physical Chemistry Chemical Physics*, **27**(29), pp. 15385-97 (2025). https://doi.org/10.1039/d5cp01585e
14. Softley, T.P. "Cold and ultracold molecules in the twenties", *Proceedings of the Royal Society A: Mathematical, Physical and Engineering Sciences*, **479**(2274), (2023). https://doi.org/10.1098/rspa.2022.0806
15. Joshi, P.R. and Lee, Y.P. "Identification of the HO˙CHC(O)NH_2 Radical intermediate in the reaction of H^+ glycolamide in solid para-hydrogen and its implication to the interstellar formation of higher-order amides and polypeptides", *ACS Earth and Space Chemistry*, **9**(3), pp. 769-781, (2025). https://doi.org/10.1021/acsearthspacechem.4c00409
16. Salta, Z., Tasinatom, N., Lupim J., et al. "Exploring the maze of $C_2N_2H_5$ radicals and their fragments in the interstellar medium with the help of quantum-chemical computations", *ACS Earth and Space Chemistry*, **4**(5), pp.774-782 (2020). https://doi.org/10.1021/acsearthspacechem.0c00062
17. Keresztes, B., Góbi, S., and Tarczay, G. "Laboratory astrochemical investigation of H-atom reactions and photochemistry of [H, C, N, S] isomers: astrophysical significance and implications", *Monthly Notices of the Royal Astronomical Society*, **527**(4), pp. 12027-43 (2024). https://doi.org/10.1093/mnras/stad3906
18. Atakan, B., Jacobs, A., Wahl, M.R., et al. "Kinetic studies of the gas phase reactions of CN with O_2 and H_2 from 294 to 1000 K", *Chemical Physics Letters*, **154**(5), pp. 449-453 (1989). https://doi.org/10.1016/0009-2614(89)87129-5
19. Zhao, G., He, M., Quan, D., et al. "Chemistry of NH_2CH_2 CH_2OH and its related species in the interstellar medium", *The Astrophysical Journal Supplement Series*, **277**(1), pp. 14 (2025). https://doi.org/10.3847/1538-4365/ada89a
20. Fereidounpour, P. and Ramazani, S. "Collision of C_2 with NH and deuterated analogs in the interstellar medium. Scattering calculations", *Molecular Physics*, **121**(6), pp. 1-15 (2023). https://doi.org/10.1080/00268976.2023.2194458
21. Sabah, A. and Ramazani, S. "A theoretical kinetic and classical dynamic investigation of CN + OH and CN + OD reactions on an interpolated potential energy surface", *Scientia Iranica*, **29**(6C), pp. 3151-3165 (2022). https://doi.org/10.24200/sci.2022.59394.6226
22. Largo, M., Sanz-Novo, M., and Redondo, P. "Formation of hydroxy, cyano and ethynyl derivatives of C4H4 isomers in the interstellar medium", *Physical Chemistry Chemical Physics*, **27**(21), pp. 11413-27 (2025). https://doi.org/10.1039/d5cp00781j
23. Cabezas, C., Agúndez, M., Endo, Y., et al. "Discovery of the interstellar cyanoacetylene radical cation HC_3N^+", *Astronomy and Astrophysics*, **687**, A48 (2024). https://doi.org/10.1051/0004-6361/202451081
24. Frisch, J., Trucs, G., Schlegel, H., et al. Gaussian 09 Program Revision C. 01. Gaussian, Inc, *Wallingford*, (2010).
25. Deegan, M.J.O. and Knowles, P.J. "Perturbative corrections to account for triple excitations in closed and open shell coupled cluster", *Chemical Physics Letters*. **227**, 321-326 (1994). https://doi.org/10.1016/0009-2614(94)00815-9
26. Moran, D., Simmonett, A.C., Leach, F.E., et al. "Popular Theoretical Methods Predict Benzene and Arenes To Be Nonplanar", *Journal of the American Chemical Society*, **128**(29), 9342-9343 (2006). https://doi.org/10.1021/ja0630285
27. Ramazani, S., Frankcombe, T.J., Andersson, S., et al. "The dynamics of the H_2 + CO+ reaction on an interpolated potential energy surface", *Journal of Chemical Physics*, **130**(24), (2009). https://doi.org/10.1063/1.479368
28. Collins, M. A. "Molecular potential-energy surfaces for chemical reaction dynamics", *Theoretical Chemistry Accounts*, **108**(6), pp. 313-24 (2002). https://doi.org/10.1007/s00214-002-0383-5
29. Thompson, K.C., Jordan, M.J.T., and Collins, M.A. "Polyatomic molecular potential energy surfaces by interpolation in local internal coordinates", *Journal of Chemical Physics*, **108**(20), pp. 8302-8316 (1998). https://doi.org/10.1063/ 1.3156805

30. Schranz, H.W., Nordholm, S., Nyman, G., et al. “An efficient microcanonical sampling procedure for molecular systems”, **1487**(1991), (2014). https://doi.org/10.1063/1.476259
31. Sharafdini, R. and Ramazani, S. “Dynamic and kinetic parameters and energy exchanges of particles in reaction of NH + OH and deuterated analogues on an Interpolated potential energy surface”, *Chemistry Select*, **5**(12), pp. 3518-3528 (2020). https://doi.org/10.1002/slct.201903596
32. Padash, R. and Ramazani, S. “Collision processes, dynamic and kinetic parameters and energy exchanges of particles in astrochemistry reaction of NH + H_2 and deuterated analogs on an interpolated potential energy surface”, *Molecular Astrophysics*, **20**, pp. 100085 (2020). https://doi.org/10.1016/j.molap.2020.100085
33. Jambrina, P.G., Menéndez, M., and Aoiz, F.J. “Angular momentum-scattering angle quantum correlation: a generalized deflection function”, *Chemical Science*, **9**(21), pp. 4837-4850 (2018). https://doi.org/10.1039/C7SC05489K
34. Ramazani, S. “Direct-dynamics VTST study of hydrogen or deuterium abstraction and C-C bond formation or dissociation in the reactions of CH_3 + CH_4, CH_3 + CD_4, CH_3D + CD_3, CH_3CH_3 + H and CH_3CD_3 + D”, *Journal of Chemical Physics*,**138**(19), pp. 1-11 (2013). https://doi.org/10.1063/1.4803862
35. Dashtaki, S.L.H. and Ramazani, S. “Variational transition state theory with multidimensional tunnelling and kinetic isotope effects in the reactions of C_2H_6, C_2H_5D and C_2D_6 with .CCl_3 to produce $CHCl_3$ and $CDCl_3$”, *Molecular Physics*, **114**(14), pp. 2195-2203 (2016). https://doi.org/10.1080/00268976.2016.1190875

Figure 1. Optimized structures of the stationary points at the QCISD(T)/6-311++G(d,p) level were show. Bond lengths were in angstroms and angles in degrees.

Figure 2. ZPE corrected relative energies of the stationary points for the reaction of CN with H_2 at the QCISD(T)/6-311++G(d,p) level of theory in kJ mol^{-1}.

Figure 3. The calculated reaction probability was presented as a function of the size of data points for the CN + H_2reaction. The initial relative translational energy was 245.7 kJ mol^{-1}.

Figure 4. The distribution of the data points from QCISD(T)/6-311++G(d,p) calculations was used for PES interpolation. The energy of each point was given relative to the energy of the reactants.

Figure 5. The reaction probability was illustrated as a function of the impact parameter for the CN + H_2 reaction, CN + DH reaction, CN + HD reaction, and CN + D_2 reaction. The relative translation energies were 245.7 kJ mol^{-1}.

Figure 6. Reaction probability was determined as a function of relative translation energy.

Figure 7. The total reaction cross-section as a function of relative translation energy.

Figure 8. Percentage of non-reactive H_2 and D_2 radicals in various scattering angles**.**

Figure 9. The scattering angle was shown as a function of the impact parameter.

Figure 10. An Arrhenius plot of the calculated rate constants was plotted for R1, R6, R11, and R16.

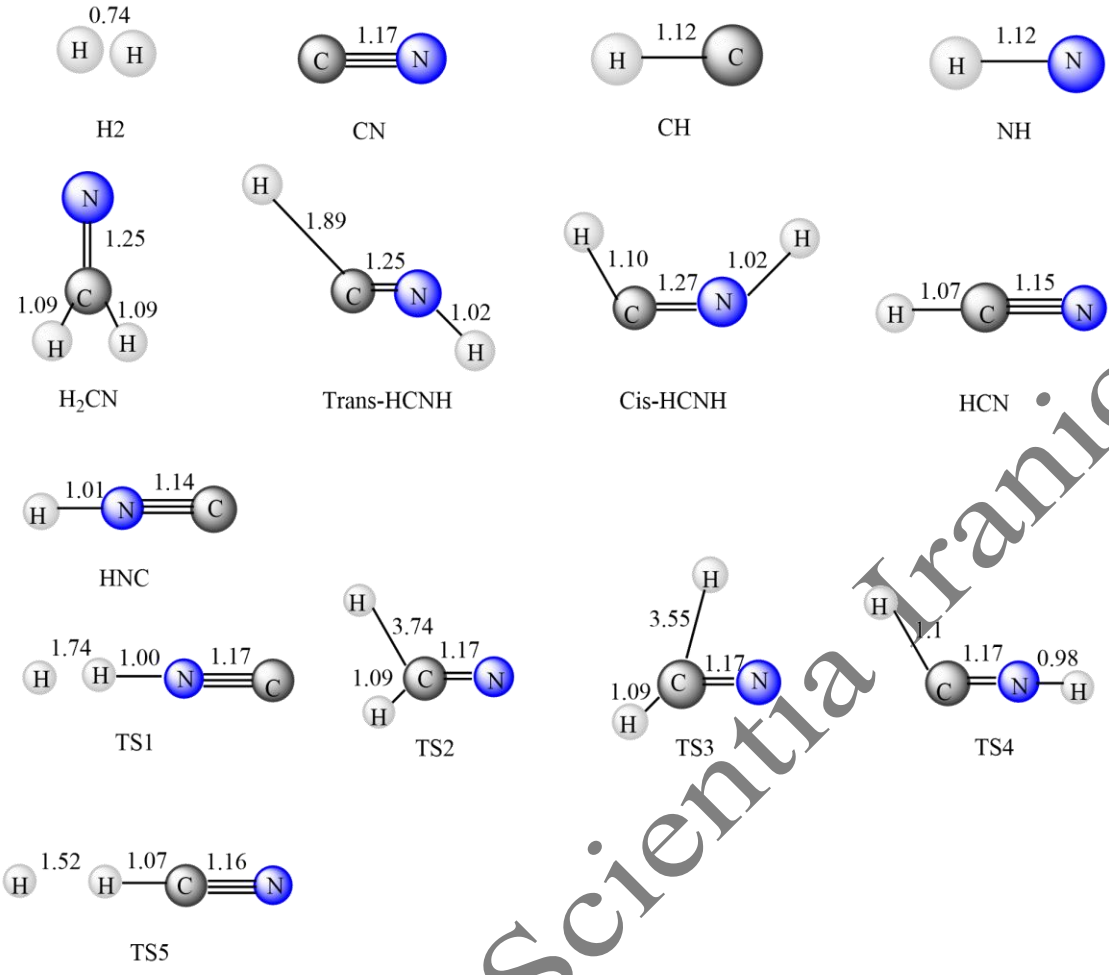

Figure 1.

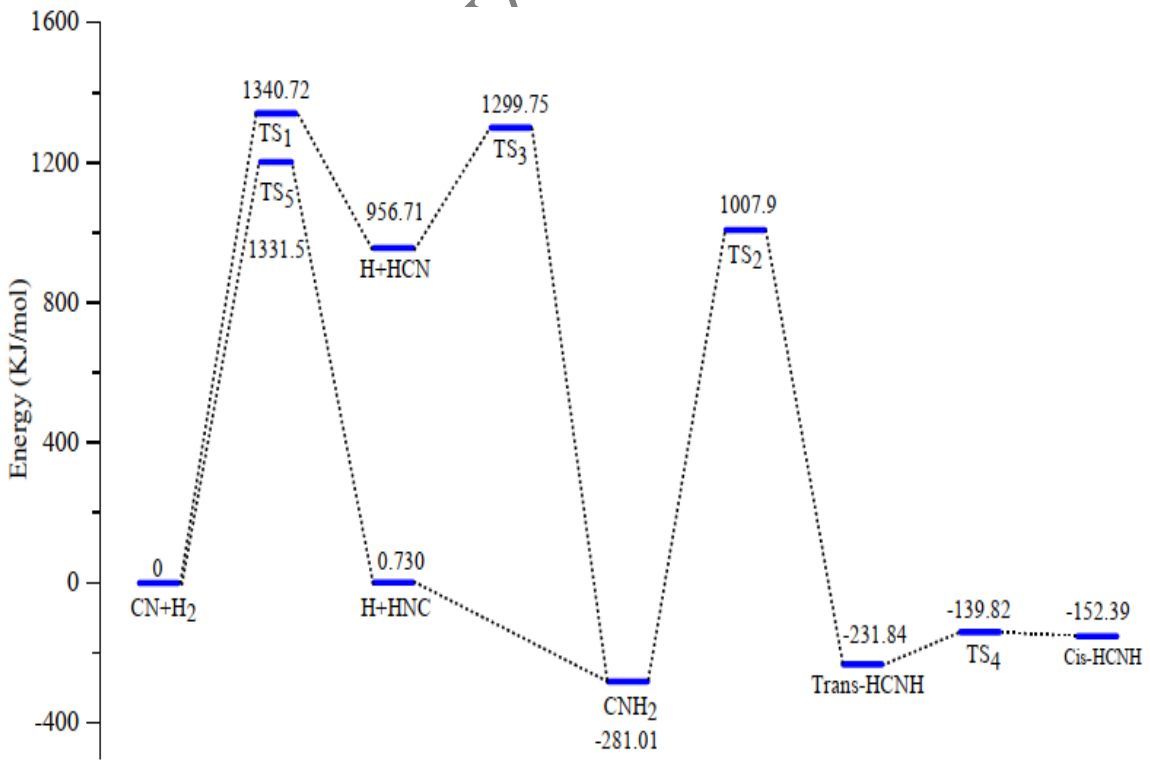

Figure 2.

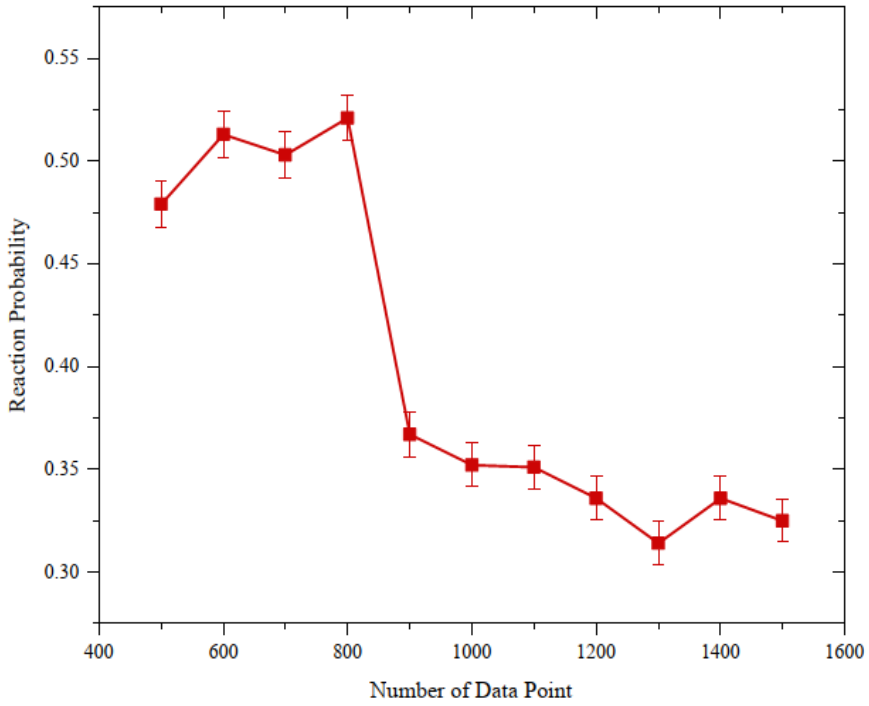

Figure 3.

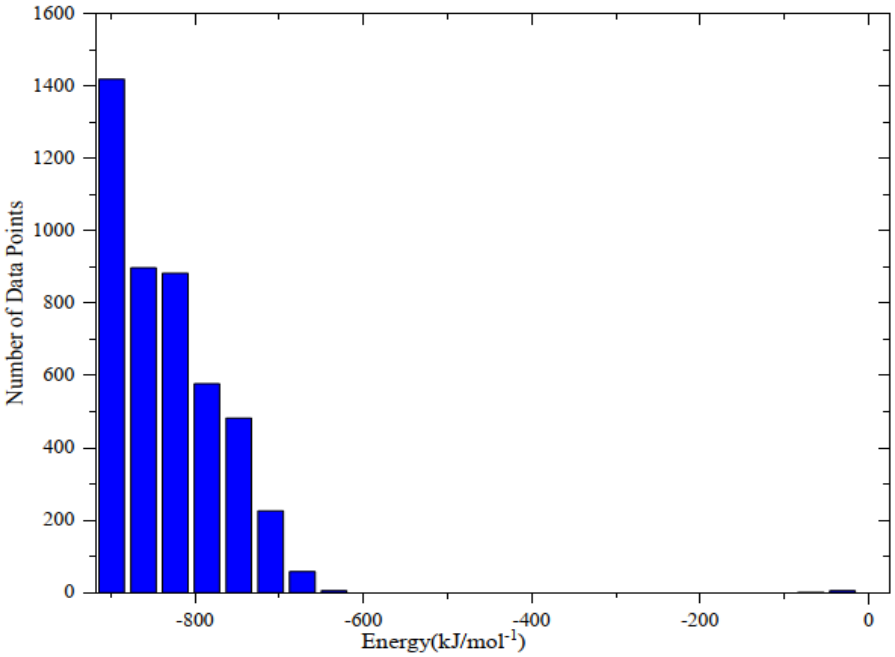

Figure 4.

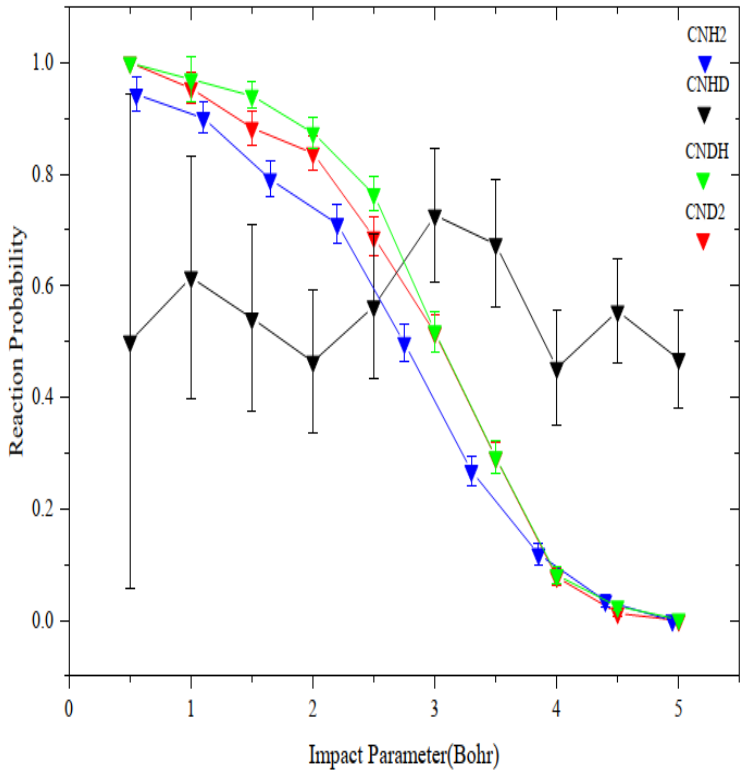

Figure 5.

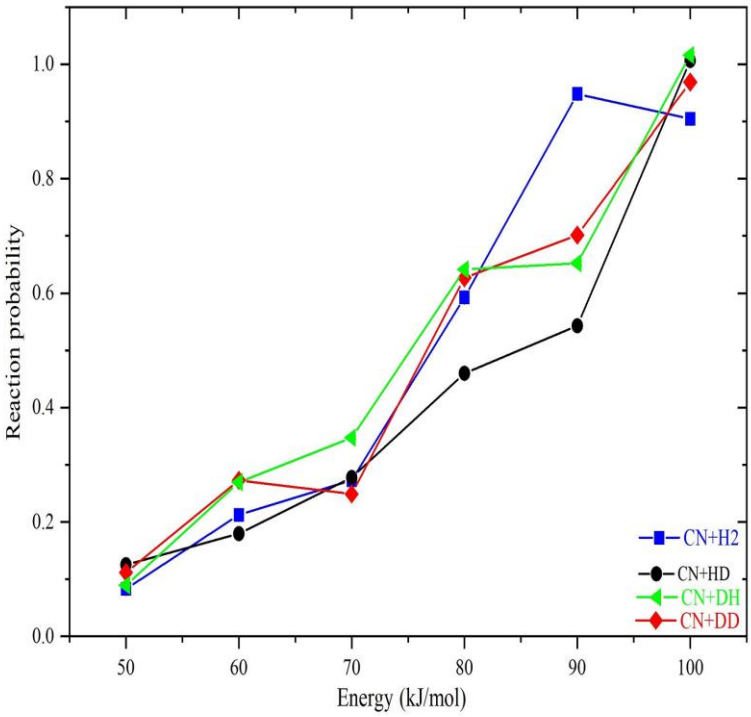

Figure 6.

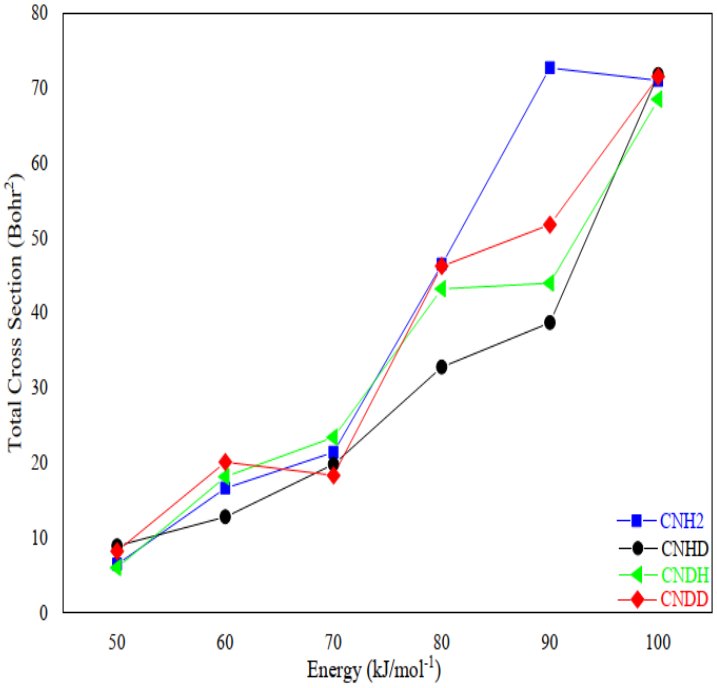

Figure 7.

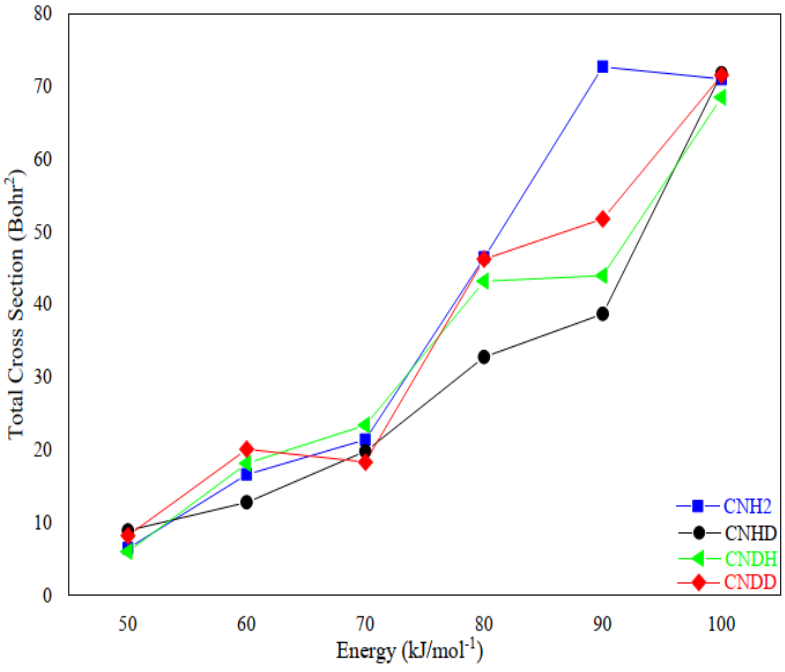

Figure 8.

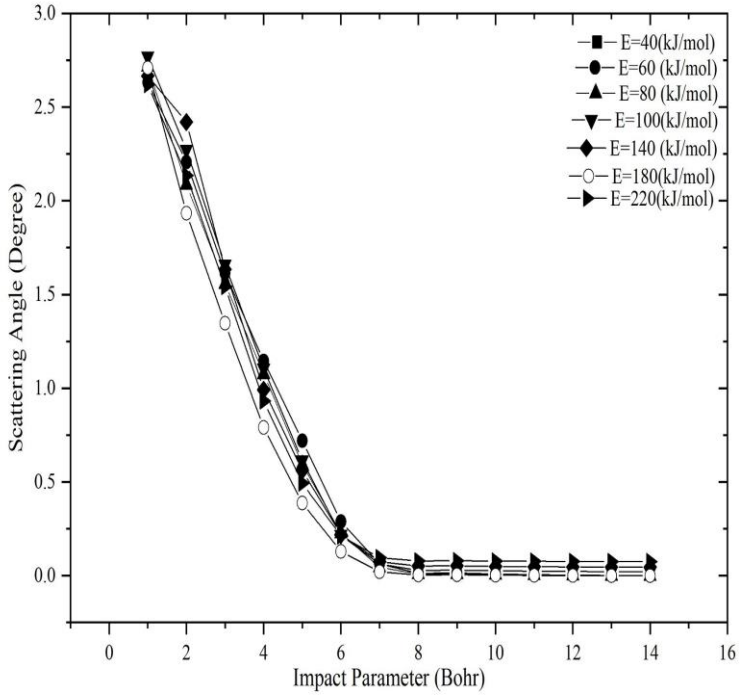

Figure 9.

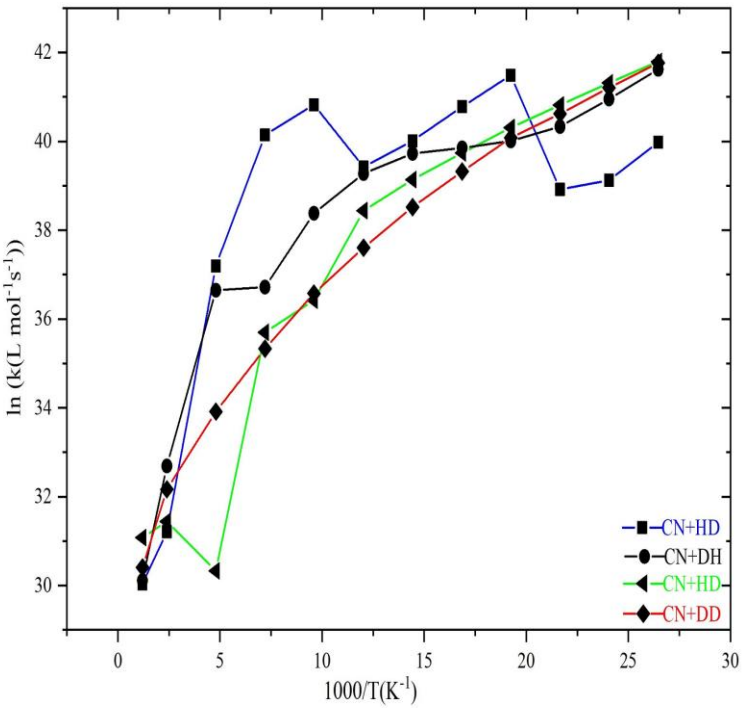

Figure 10.

Table 1. Scattering angle expressions in the various relative translational energies.

$E(kJ\ mol^{-1})$	$b < d_{CNH_2}$	$b > d_{CNH_2}$
40	$\theta = 3.120 - 0.4486b$	$\theta = 0.0465 - 0.0034b$
	$1 \le b \le 7$	$7 \le b \le 14$
60	$\theta = 3.014 - 0.4440b$	$\theta = 0.0334 - 0.0024b$
	$1 \le b \le 7$	$7 \le b \le 14$
80	$\theta = 2.9990 - 0.4534b$	$\theta = 0.0232 - 0.0017b$
	$1 \le b \le 7$	$7 \le b \le 14$
100	$\theta = 2.878 - 0.4376b$	$\theta = 0.0181 - 0.0013b$
	$1 \le b \le 7$	$7 \le b \le 14$
120	$\theta = 2.599 - 0.4005b$	$\theta = 0.0138 - 0.0010b$
	$1 \le b \le 7$	$7 \le b \le 14$
140	$\theta = 2.850 - 0.4511b$	$\theta = 0.0098 - 0.0007b$
	$1 \le b \le 7$	$7 \le b \le 14$

Table 2. The fitted parameters using $\sigma(E) = aE^{\gamma}$.

	a	γ	$\Gamma(\gamma+2)$	$k(T)$ L mol^{-1}s^{-1}
H_2H_2	0.0002	2.8606	19.49	$6.22\times10^{2}\times T^{3.36}$
HD	8.66	3.53	54.93	$2.19\times10^{4}\times T^{4.03}$
DH	2.71	2.76	16.85	$1.55\times10^{5}\times T^{3.26}$
D_2	1.623	2.837	18.83	$3.77\times10^{4}\times T^{3.33}$

Table 3. The primary kinetic isotope effect on the rate constant and reaction cross-section calculations.

E kJ mol^{-1}	40	60	80	100	120	140
k_1 / k_6	1.225	1.224	1.223	1.225	1.966	1.965
k_1 / k_{11}	1.318	1.237	1.279	1.311	1.283	1.245
k_1 / k_{16}	1.347	1.751	1.616	1.332	1.355	1.300
∂_1/∂_6	3.69	5.33	3.35	1.39	4.47	1.19
∂_1/∂_{11}	7.45	7.28	3.66	1.28	3.58	8.52
∂_1/∂_{16}	1.650	1.660	8.58	3.06	8.65	2.08
$\eta_{trans}(R_1 / R_6)$	1.398	1.398	1.398	1.398	1.398	1.398
$\eta_{trans}(R_1 / R_{11})$	1.398	1.398	1.398	1.398	1.398	1.398
$\eta_{trans}(R_1 / R_{16})$	1.026	1.026	1.026	1.026	1.026	1.026